Phase diagram of the one-dimensional $S=\frac{1}{2}$ *XXZ* model with ferromagnetic nearest-neighbor and antiferromagnetic next-nearest-neighbor interactions

R. Jafari[1] and A. Langari[2,3]
[1]*Institute for Advanced Studies in Basic Sciences, P.O. Box 45195-1159, Zanjan, Iran*
[2]*Department of Physics, Sharif University of Technology, 14588-89694, Tehran, Iran*
[3]*Institute for Studies in Theoretical Physics and Mathematics (IPM), Tehran 19395-5531, Iran*
(Received 17 January 2007; revised manuscript received 30 May 2007; published 10 July 2007)

We have studied the phase diagram of the one-dimensional $S=\frac{1}{2}$ *XXZ* model with ferromagnetic nearest-neighbor and antiferromagnetic next-nearest-neighbor interactions. We have applied the quantum renormalization group (QRG) approach to obtain stable fixed points and the scaling of coupling constants. The QRG prescription has to be implemented to the second order of interblock interactions to obtain a self-similar Hamiltonian after each step of the QRG. This model shows a rich phase diagram which includes quantum spin-fluid and dimer phases in addition to the classical Néel and ferromagnetic ones. We have found the border between different phases by tracing the scaling of coupling constants.

DOI: 10.1103/PhysRevB.76.014412 PACS number(s): 75.10.Jm, 75.10.Pq, 75.30.Kz

I. INTRODUCTION

There is currently much interest in quantum spin systems that exhibit frustrations. This has been simulated in particular by study of the magnetic properties of the cuprates which become high-T_c superconductors when doped. Frustrated spin systems are known to have many interesting properties which are quite different from those of conventional magnetic systems.

The Heisenberg spin-$\frac{1}{2}$ chain with nearest-neighbor (NN) and next-nearest-neighbor (NNN) interactions (which is equivalent to a zigzag ladder) is a typical model with frustrations. In recent years, several interesting quasi-one-dimensional magnetic systems have been studied experimentally.[1–3] Among them, some compounds containing CuO chains with edge-sharing CuO_4 plaquettes were expected to be described by the *XXZ* model with next-nearest-neighbor interactions. The nearest-neighbor (Cu-Cu) spin interaction changes from antiferromagnetic (AFM) to ferromagnetic (FM), as the angle θ of the Cu-O-Cu bound approaches 90°. The next-nearest-neighbor interaction is always AFM and is not dependent on θ.[4] Several compounds with edge-sharing chains are known, such as Li_2CuO_2, $La_6Ca_8Cu_{21}O_{41}$, $Ca_2Y_2Cu_5O_{10}$, and $Rb_2Cu_2Mo_3O_{12}$, which can be considered as an ideal model compounds with the ferromagnetic NN interactions and antiferromagnetic NNN interactions.[5,6]

The general Hamiltonian of such models on a periodic chain of N sites is

$$H=\frac{J}{4}\left\{\sum_{i=1}^{N}(\sigma_i^x\sigma_{i+1}^x+\sigma_i^y\sigma_{i+1}^y+\Delta\sigma_i^z\sigma_{i+1}^z)+\sum_{i=1}^{N}J_2(\sigma_i^x\sigma_{i+2}^x+\sigma_i^y\sigma_{i+2}^y+\delta\sigma_i^z\sigma_{i+2}^z)\right\},\qquad(1)$$

where J and J_2 are the first- and second-nearest-neighbor exchange couplings and the corresponding easy-axis anisotropies are defined by Δ and $\Delta_2=J_2\delta$. For a chain of only NN interactions ($J_2=0$) the ground-state properties are well known from the Bethe ansatz.[7] Adding the NNN interaction will change the ground-state behavior. The case of positive coupling constants (J, J_2, Δ, $\delta>0$) has been investigated by several authors.[8–18] In particular, it has been shown that a transition from a gapless state to a dimerized one takes place at ($J_2=0.24$, $\Delta=\delta=1$).[8] The point ($J_2=\frac{1}{2}$, $\Delta=\delta=1$) corresponds to the well-known Majumdar-Ghosh model where the exact ground state is constructed from the direct products of dimers which leads to a gapful phase.[10]

Relatively less is known about the model with ferromagnetic NN ($J<0$) and antiferromagnetic NNN ($JJ_2>0$) interactions. Though this model has been a subject of many studies,[15–26] a complete picture of the phases in this model is still being sought.[21] It is well known that there is a critical point ($J_2=\frac{1}{4}$, $\Delta=-\delta=-1$) where the ferromagnetic state is unstable and the ground state is nontrivial at $J_2>\frac{1}{4}$ which can be realized by different phases.[22] Moreover, the exact ground state can be represented in the resonating valence bound state (RVB).[23,24] This state has been proposed as a candidate for the spin-liquid ground state.[27] One of the most important and open questions is the possibility of the spontaneous dimerization of the system in the singlet phase accompanied by a gap in the spectrum.[25] A controversial conclusion exists about the presence of a gap at $J_2>\frac{1}{4}$. It has long been believed that the model is gapless[13,26] but one-loop renormalization group analysis shows[15,28] that the gap opens due to a Lorentz-symmetry-breaking perturbation. However, the presence of a gap is not obvious from the numerical data, because the excitation energy values fit to $\frac{1}{N}$ (N is the chain length) which is evidence for a gapless behavior.[15] On the basis of field theory considerations it was proposed[16] that a very tiny but finite gap exists which cannot be observed numerically.

We have considered the one-dimensional anisotropic $S=\frac{1}{2}$ Heisenberg model with ferromagnetic NN and antiferromagnetic NNN interactions by implementing the quantum renormalization group (QRG) method. We have calculated the effective Hamiltonian up to second-order corrections. A second-order correction is necessary to be taken into account

to obtain a self-similar Hamiltonian after each step of the QRG. In this approach, we have considered the effect of whole states of the block Hamiltonian which are partially ignored in the first-order approach. The present scheme allows us to have analytic RG equations, which give a better understanding of the behavior of the system by the scaling of coupling constants. We have succeeded in obtaining a phase diagram in good qualitative agreement with the numerical ones.[17]

We have previously studied the antiferromagnetic model ($J>0$, $J_2>0$) in Eq. (1) for $\Delta>0$ by the QRG method.[14] For $0\leq\Delta<1$ the interplay of the two competing terms (NN and NNN) in the presence of quantum fluctuations produces the dimer phase for $J_2\geq J_2^c(\Delta,\Delta_2)$. The dimer or spin Peierls phase has a spin gap and a broken translation symmetry (the unit cell is doubled) in the thermodynamic limit. However, we have determined the fluid-dimer phase transition by using the scaling of couplings under the RG (see Fig. 3 of Ref. 14 or the complete phase diagram presented in Fig. 3 in this article). In the spin-fluid phase, the anisotropy and next-nearest-neighbor couplings are irrelevant while in the dimer phase they run to the triple point ($\Delta_2^*=J_2^*\simeq 0.155$, $\Delta^*=1$). From a quantitative point of view at $\Delta=0$ the RG analysis gives $J_2^c\simeq 0.44$ which can be compared with the numerical result of $J_2^c\simeq 0.33$ presented in Ref. 9. The Néel phase appears just by crossing the $\Delta=1$ plane at $\Delta_2=0$ and $J_2=0$. In the $\Delta_2=0$ plane and for $\Delta>1$, the model will pass through a phase transition from Néel to dimer phase for $J_2>J_2^c(\Delta)$. The Néel order is also broken by increasing the anisotropy of the NNN interaction.

In this paper we will complete the phase diagram of this model for the whole range of parameters. We intend to consider the *XXZ* model with ferromagnetic NN ($J<0$) and antiferromagnetic NNN ($JJ_2>0$) interactions which can be fulfilled by extending the phase diagram to $J<0$ and $JJ_2>0$. To do so, we simply make the following rotation which maps the ferromagnetic case ($J<0$, $\Delta>0$) to the antiferromagnetic one ($J>0$) with negative anisotropy ($\Delta<0$). The other couplings in Eq. (1) (J_2, δ) remain unchanged. If we implement a π rotation around the z axis for the even sites and leave the odd sites unchanged, the Hamiltonian (with $J<0$ and $JJ_2>0$) is transformed into the following form:

$$H=\frac{J}{4}\left\{\sum_{i=1}^{N}(\sigma_i^x\sigma_{i+1}^x+\sigma_i^y\sigma_{i+1}^y-\Delta\sigma_i^z\sigma_{i+1}^z)+\sum_{i=1}^{N}J_2(\sigma_i^x\sigma_{i+2}^x+\sigma_i^y\sigma_{i+2}^y+\delta\sigma_i^z\sigma_{i+2}^z)\right\},\quad J,J_2,\Delta,\delta>0. \tag{2}$$

The QRG procedure is implemented on the rotated Hamiltonian [Eq. (2)] which makes the calculations easier. However, the phase diagram and other figures presented in this article are based on the couplings defined in Eq. (1) where negative NN anisotropy ($\Delta<0$) corresponds to the ferromagnetic NN case ($J<0$).

The QRG approach will be explained in the next section where the second-order effective Hamiltonian and the renormalization of the coupling constants are obtained. In Sec. III, we will present the phase diagram and its characteristics where a comparison with numerical results is done.[17] Finally, we summarize our results.

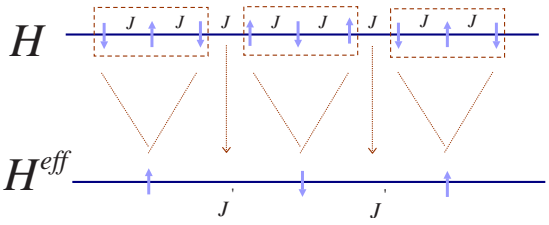

FIG. 1. (Color online) The decomposition of a chain into a three-site block Hamiltonian (H^B) and interblock Hamiltonian (H^{BB}).

II. RG EQUATIONS

The main idea of the QRG method is the mode elimination or thinning of the degrees of freedom followed by an iteration which reduces the number of variables step by step until a more manageable situation is reached. We have implemented Kadanoff's block method for this purpose, because it is well suited to perform analytical calculations in the lattice models and it is conceptually easy to extend to higher dimensions.[29–32] In Kadanoff's method, the lattice is divided into blocks where the Hamiltonian is exactly diagonalized. By selecting a number of low-lying eigenstates of the blocks the full Hamiltonian is projected onto these eigenstates which gives the effective (renormalized) Hamiltonian. The effective Hamiltonian up to second-order corrections is[14,29,30]

$$H^{eff}=H_0^{eff}+H_1^{eff}+H_2^{eff},$$

$$H_0^{eff}=P_0H^BP_0,\quad H_1^{eff}=P_0H^{BB}P_0,$$

$$H_2^{eff}=P_0\left[H^{BB}(1-P_0)\frac{1}{E_0-H^B}(1-P_0)H^{BB}\right]P_0.$$

We have applied the mentioned scheme to the Hamiltonian defined in Eq. (2). We have considered a three-site block procedure defined in Fig. 1. The block Hamiltonian ($H^B=\Sigma h_I^B$) of the three sites and its eigenstates and eigenvalues are given in Appendix A. The three-site block Hamiltonian has four doubly degenerate eigenvalues (see Appendix A). P_0 is the projection operator of the ground-state subspace which is defined by

$$P_0=|\Uparrow\rangle\langle\psi_0|+|\Downarrow\rangle\langle\psi_0'|. \tag{3}$$

In Eq. (3), $|\psi_0\rangle$ and $|\psi_0'\rangle$ are doubly degenerate ground states which are explicitly represented in Appendix A. Moreover, $|\Uparrow\rangle$ and $|\Downarrow\rangle$ are the renamed base kets which define the Hilbert space of the renormalized (new) site after the QRG step. We have kept two states ($|\psi_0\rangle$ and $|\psi_0'\rangle$) for each block to define the effective (new) site. Thus, the effective site can be considered as a spin 1/2. Due to the level crossing which occurs for the eigenstates of the block Hamiltonian, the projection operator (P_0) can be different depending on the coupling constants. Therefore, we must specify the regions with

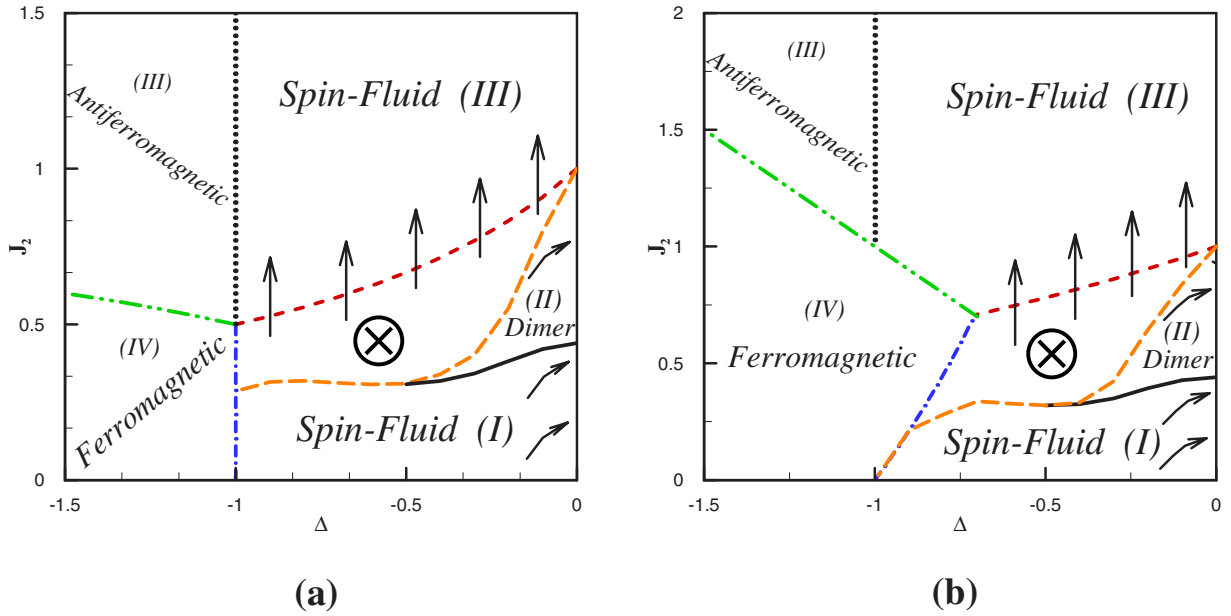

FIG. 2. (Color online) The cross section of the three-dimensional phase diagram for $\Delta<0$. (a) The crossed plane is $\Delta_2=J_2\Delta$ and (b) $\Delta_2=0$.

the corresponding ground states. The eigenvalues of the block Hamiltonian are labeled by e_0, e_1, e_2, and e_3 (see Appendix A). In the following, we will classify the regions where each of this states represent the ground state. A summary of this information is given in Fig. 4 in Appendix A.

A. Region (A): e_0 as the ground-state energy

In this region the effective Hamiltonian in the first-order correction leads to an XXZ chain without the NNN interaction ($J_2'=0$); i.e., the effective Hamiltonian is not exactly similar to the initial one. The NNN interaction is the result of the second-order correction. When the second-order correction is added to the effective Hamiltonian, the renormalized Hamiltonian, apart from an additive constant, is similar to Eq. (2) with the renormalized couplings. Thus, the effective Hamiltonian including the second-order correction for $\Delta>0$ is

$$H^{eff}=\frac{J'}{4}\left[\sum_i^{N/3}(\sigma_i^x\sigma_{i+1}^x+\sigma_i^y\sigma_{i+1}^y)-\Delta'(\sigma_i^z\sigma_{i+1}^z)+\sum_i^{N/3}J_2'(\sigma_i^x\sigma_{i+2}^x+\sigma_i^y\sigma_{i+2}^y)+\Delta_2'(\sigma_i^z\sigma_{i+2}^z)\right].$$

The renormalized coupling constants are functions of the original ones which are given in Appendix B.

B. Region (B): e_2 as the ground-state energy

The second-order effective Hamiltonian is similar to the case of region (A) with different coupling constants given in Appendix C. A note is in order here: although the second-order correction is necessary to produce the NNN interaction in the effective Hamiltonian, the initial values of $J_2=0$ and $\Delta_2=0$ do not produce NNN interactions. It is different from the RG flow obtained in region (A).

C. Region (C): e_3 as the ground-state energy

In this region the effective Hamiltonian to the second-order corrections leads to the Ising model

$$H^{eff}=\frac{1}{4}\left[\sum_i^{N/3}-\Delta'(\sigma_i^z\sigma_{i+1}^z)\right], \tag{4}$$

where

$$\Delta'=J(\Delta+2\Delta_2)+\frac{J^2}{4}\left[\left(\frac{1}{e_3-e_0}\right)\left(\frac{1}{2+q^2}\right)(1+2J_2q)^2+\left(\frac{1}{e_3-e_1}\right)\left(\frac{1}{2+p^2}\right)(1+2J_2p)^2+\left(\frac{1}{e_3-e_2}\right)\left(\frac{1}{2}\right)^2\right]+J^2\left[\left(\frac{1}{2e_3-e_1-e_0}\right)\left(\frac{1}{2+q^2}\right)\left(\frac{1}{2+p^2}\right)(1+2J_2(p+q))^2+\left(\frac{1}{2e_3-e_2-e_0}\right)\left(\frac{1}{2+q^2}\right)\left(\frac{1}{2}\right)(1+2J_2q)^2+\left(\frac{1}{2e_3-e_2-e_1}\right)\left(\frac{1}{2+p^2}\right)\left(\frac{1}{2}\right)(1+2J_2p)^2\right].$$

This simply introduces the ferromagnetic behavior. We will discuss the phase diagram in terms of different regions defined above in the following section.

III. PHASE DIAGRAM

A. Region (A)

In the $\Delta<0$ case, the RG equation shows scaling of J to zero which represents the renormalization of the energy

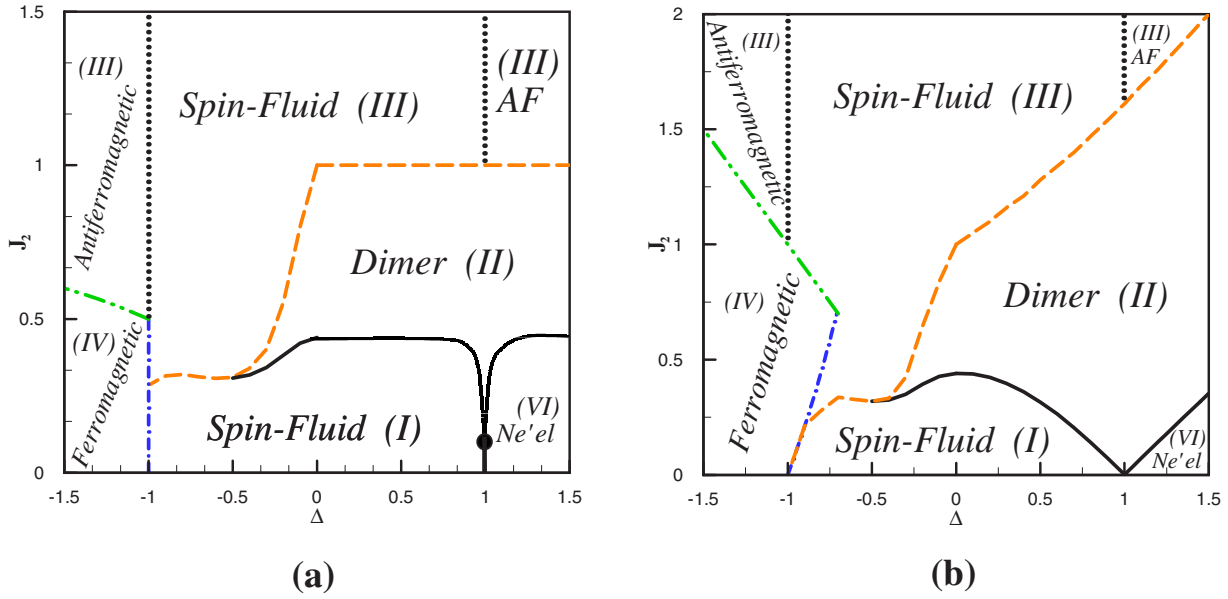

FIG. 3. (Color online) The projection of the complete phase diagram on the $\Delta 2=J_2\Delta$ plane in (a) and on the $\Delta_2=0$ plane in (b).

scale. We have plotted the RG flow and different phases in Fig. 2. The solid line is the boundary between dimer (II) phase and spin-fluid (I) phase. If we start from the spin-fluid (I) phase or dimer (II) phase, the sign of NN anisotropy (Δ) changes under the RG after few steps. However, in the dimer (II) phase the amount of NNN coupling (J_2) is greater than 0.44 just when the anisotropy changes sign, while in the spin-fluid (I) phase it is less than 0.44. In other words, in the dimer (II) phase the RG flow goes to the triple point ($\Delta_2^*=J_2^*\simeq 0.155$, $\Delta^*=1$) (solid circle in Fig. 3) while it goes to the $\Delta=J_2=\Delta_2=0$ fixed point starting from the spin-fluid (I) phase. The spin-fluid (I) phase is represented by the NN *XX*spin-1/2 Hamiltonian in the stable fixed point,

$$H^*_{spin\ fluid(I)}=\sum_i(\sigma_i^x\sigma_{i+1}^x+\sigma_i^y\sigma_{i+1}^y), \tag{5}$$

while the corresponding fixed-point Hamiltonian for the dimer (II) phase is

$$H^*_{dimer(II)}=\sum_i(\sigma_i^x\sigma_{i+1}^x+\sigma_i^y\sigma_{i+1}^y+\sigma_i^z\sigma_{i+1}^z)+J_2^*\sum_i(\sigma_i^x\sigma_{i+2}^x+\sigma_i^y\sigma_{i+2}^y+\sigma_i^z\sigma_{i+2}^z). \tag{6}$$

In Figs. 2(a) and 2(b) the black arrows show the scaling of couplings under the RG. In the region denoted by $\otimes$, although e_0 is the ground-state energy, the behavior of the couplings constant is not the same as the couplings in the dimer (II) phase. In this region ($\otimes$) the coupling constants go to the spin-fluid (III) phase. It means that the region denoted by $\otimes$ and spin-fluid (III) are a unique phase. The spin-fluid (III) phase is represented by two isolated chains with NN *XX* interactions. The two chains are composed by odd and even sites of the original Hamiltonian where the NN interaction between odd and even ones has been scaled to zero and only the NNN interaction between odd or even sites remains finite. The fixed point of spin-fluid (III) can be represented by the following Hamiltonian where the site index ($i=2m$ or $2m+1$, m is any integer) refers to the original chain:

$$H^*_{spin\ fluid(III)}=\sum_i(\sigma_i^x\sigma_{i+2}^x+\sigma_i^y\sigma_{i+2}^y). \tag{7}$$

The authors in Ref. 17 were not able to specify the phase of this region numerically. We denote the boundary between the spin-fluid (III) and both dimer (II) and spin-fluid (I) phases by long-dashed lines. The dashed line behind the arrows is not a phase boundary and just represents the two regions with different ground states (see Appendix A).

It is known that on the $\Delta_2=J_2\Delta$ plane and $\Delta=-1$ there is a fixed point: namely, $\Delta=-1$, $J_2=0.25$.[23,24] However, our approach is not able to show this fixed point because this is on the plane which is separated by spin-fluid (I) and ferromagnetic phases where the level crossing occurs. Instead, close to the $\Delta=-1$ line ($\Delta\gtrsim -1$) we found the critical value of $J_2^c=0.28$ which distinguishes the spin-fluid (I) and spin-fluid (III) phases.

B. Region (B)

In this region the NNN interactions are greater than NN interactions. The implementation of bosonization technique combined with a mean-field analysis in Ref. 28 predicted that for the $\Delta_2=J_2\Delta$ plane and $\Delta=0$, the system might exhibit a chiral-ordered phase with gapless excitations where $J_2>J_2^c=1.26$. The predicted critical value (J_2^c) is in good agreement with the numerical density matrix renormalization group result.[18] Our approach shows that all coupling constants are irrelevant except J_2 and Δ_2. For $-1<\Delta<0$ the ratio of Δ_2/J_2 goes to zero, and for $\Delta<-1$ this ratio goes to infinity. It means that in the fixed point of this region the original spin chain decouples to two *XXZ* chains without next-nearest-neighbor interactions where the lattice spacing is doubled. For $-1<\Delta<0$, the model is in the spin-fluid (III) phase ($\Delta_2=0$) which is specified in Fig. 2 and represented by

the fixed-point Hamiltonian, Eq. (7). The spin-fluid (III) phase is different from the spin-fluid (I) phase according to their stable fixed points. The stable fixed point for the spin-fluid (I) phase is $J_2=0$, $\Delta_2=0$ and $\Delta=0$ while for the spin-fluid (III) phase all couplings are zero except J_2. Note that the level crossing of e_0 and e_2 does not define the border between spin-fluid (III) and dimer (II) phases. This border is defined by the scaling of couplings under RG equations. For $\Delta<-1$ the model is in the antiferromagnetic phases. In this case the model is decoupled to two antiferromagnetic Ising chains. Thus the ground state is long-range antiferromagnetic ordered $|\uparrow\uparrow\downarrow\downarrow\uparrow\uparrow\downarrow\downarrow\cdots\rangle$.

C. Region (C)

As we pointed out in Sec. II C, even after adding second-order corrections, the original Hamiltonian is mapped to the ferromagnetic Ising model [Eq. (4)]. The Ising model remains unchanged under the RG because it is a fixed point and its properties are well known. We call this region as the ferromagnetic phase.

IV. SUMMARY AND DISCUSSIONS

We mapped the one-dimensional ferromagnetic NN and antiferromagnetic NNN $S=\frac{1}{2}$ XXZ model to the antiferromagnetic model in Eq. (2) with negative anisotropy. We have implemented the second-order QRG procedure to obtain the phase diagram of this model. The complete phase diagram which also covers the positive anisotropy region is presented in Fig. 3. This is a cross section of the phase diagram with $\Delta_2=J_2\Delta$ plane in Fig. 3(a) and with $\Delta_2=0$ plane in Fig. 3(b). For $-0.5<\Delta<1$ (on the $\Delta_2=J_2\Delta$ plane), when J_2 is smaller than the critical value (J_2^c), the system is in the gapless spin-fluid (I) phase. By contrast, for larger value of $J_2>J_2^c$ the system is in the dimer phase with a finite energy gap above the doubly degenerate ground states (the transition is denoted by solid line). As J_2 increases, the system exhibits a transition from the dimer phase to the spin-fluid (III) phase which is called the gapless chiral phase in Ref. 18. The transition is denoted by the long-dashed line in the phase diagram. The transition takes place at $J_2^c=1$ for $\Delta=0$, in qualitative agreement with $J_2^c=1.26$ of Ref. 18. For $-1<\Delta<-0.5$ (on the $\Delta_2=J_2\Delta$ plane) at J_2^c a transition occurs from the spin-fluid(I) to spin-fluid (III) (chiral order) phases. The QRG equations for $\Delta\gtrsim-1$ shows a critical line (long-dashed line) which separates the spin-fluid (I) and spin-fluid (III) phases without an intermediate region. Thus, we claim that for $J_2>J_2^c=0.28$ there is no gap and the model is not in the dimer phase. The model is in the ferromagnetic phase where $\Delta<-1$ and small J_2. The phase transition to the long-range antiferremagnetic phase takes place at $J_2>J_2^c$ (dash-double-dotted line). In the case of $\Delta>1$, a transition from the Néel (VI) phase to the dimer phase occurs as J_2 increases (solid line). The dimer phase is unstable by increasing J_2 further which leads to a transition to the antiferromagnetic [AF(III)] phase (long-dashed line). However, the comparison of Fig. 3(a) with 3(b) shows that the anisotropy of the NNN term (Δ_2) changes the phase diagram significantly. From the parameters estimated for several compounds near the isotropic limit ($\Delta=1$, $\Delta_2=J_2\Delta$), $La_6Ca_8Cu_{21}O_{41}$ ($J_2^c=0.36$), Li_2CuO_2 ($J_2^c=0.62$), and $Ca_2Y_2Cu_5O_{10}$ ($J_2^c=2.2$),[4] our results predict for $\Delta>-1$ that all of them are in the chiral order phase [spin-fluid (III)] without a gap, and for $\Delta<-1$, $La_6Ca_8Cu_{21}O_{41}$ is in the ferromagnetic phase and Li_2CuO_2 and $Ca_2Y_2Cu_5O_{10}$ are in long-range antiferromagnetic order.

ACKNOWLEDGMENTS

The authors would like to thank M. R. H. Khajehpour for a careful reading of the manuscript and fruitful discussions. This work was partially supported by the Center for Excellence in Complex Systems and Condensed Matter at Sharif University of Technology.

APPENDIX A: THE BLOCK-HAMILTONIAN OF THREE SITES AND ITS EIGENVECTORS AND EIGENVALUES

We have considered the three-site block (Fig. 1) with the following Hamiltonian:

$$h_I^B=\frac{J}{4}[(\sigma_{1,I}^x\sigma_{2,I}^x+\sigma_{2,I}^x\sigma_{3,I}^x+\sigma_{1,I}^y\sigma_{2,I}^y+\sigma_{2,I}^y\sigma_{3,I}^y)-\Delta(\sigma_{1,I}^z\sigma_{2,I}^z+\sigma_{2,I}^z\sigma_{3,I}^z)+J_2(\sigma_{1,I}^x\sigma_{3,I}^x+\sigma_{1,I}^y\sigma_{3,I}^y)+\Delta_2(\sigma_{1,I}^z\sigma_{3,I}^z)],$$

where $\sigma_{j,I}^{\alpha}$ refers to the α component of the Pauli matrix at site j of the block labeled by I. The exact treatment of this Hamiltonian leads to four distinct eigenvalues which are doubly degenerate. The ground, first, second, and third excited-state energies have the following expressions in terms of the coupling constants:

$$|\psi_0\rangle=\frac{1}{\sqrt{2+q^2}}(|\uparrow\uparrow\downarrow\rangle+q|\uparrow\downarrow\uparrow\rangle+|\downarrow\uparrow\uparrow\rangle),$$

$$|\psi_0'\rangle=\frac{1}{\sqrt{2+q^2}}(|\uparrow\downarrow\downarrow\rangle+q|\downarrow\uparrow\downarrow\rangle+|\downarrow\downarrow\uparrow\rangle),$$

$$e_0=\frac{J}{4}[J_2+\Delta-\sqrt{(J_2-\Delta-\Delta_2)^2+8}],$$

$$|\psi_1\rangle=\frac{1}{\sqrt{2+p^2}}(|\uparrow\uparrow\downarrow\rangle+p|\uparrow\downarrow\uparrow\rangle+|\downarrow\uparrow\uparrow\rangle),$$

$$|\psi_1'\rangle=\frac{1}{\sqrt{2+p^2}}(|\uparrow\downarrow\downarrow\rangle+p|\downarrow\uparrow\downarrow\rangle+|\downarrow\downarrow\uparrow\rangle),$$

$$e_1=\frac{J}{4}[J_2+\Delta+\sqrt{(J_2-\Delta-\Delta_2)^2+8}],$$

$$|\psi_2\rangle=\frac{1}{\sqrt{2}}(|\downarrow\downarrow\uparrow\rangle-|\uparrow\downarrow\downarrow\rangle),\quad |\psi_2'\rangle=\frac{1}{\sqrt{2}}(|\uparrow\uparrow\downarrow\rangle-|\downarrow\uparrow\uparrow\rangle),$$

$$e_2=\frac{-J}{4}(2J_2+\Delta_2),$$

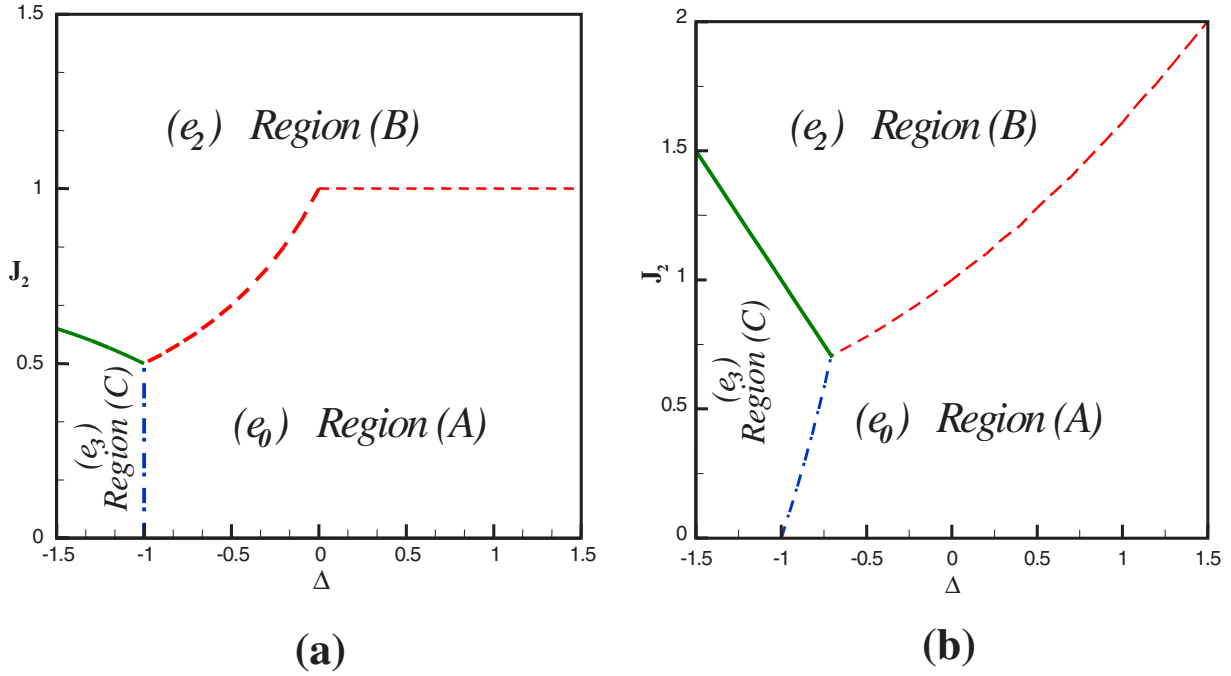

FIG. 4. (Color online) The projection of the three-dimensional border areas on the $\Delta 2=J_2\Delta$ plane (a) and for $\Delta_2=0$ plane in (b).

$$|\psi_3\rangle = |\uparrow\uparrow\uparrow\rangle, \quad |\psi_3'\rangle = |\downarrow\downarrow\downarrow\rangle,$$

$$e_3 = \frac{J}{4}(\Delta_2 - 2\Delta),$$

where q and p are

$$q = \frac{-1}{2}[J_2 - \Delta - \Delta_2 + \sqrt{(J_2 - \Delta - \Delta_2)^2 + 8}],$$

$$p = \frac{-1}{2}[J_2 - \Delta - \Delta_2 - \sqrt{(J_2 - \Delta - \Delta_2)^2 + 8}].$$

$|\uparrow\rangle$ and $|\downarrow\rangle$ are the eigenstates of σ^z.

In Fig. 4 we present the different regions where the specified state is the ground state of the block Hamiltonian. The border between these regions is specified as a projection on to a fixed plane. The projection on to the $\Delta_2=J_2\Delta(\Delta=\delta)$ plane is shown in Fig. 4(a) and the projection on to the $\Delta_2=0$ plane is plotted in Fig. 4(b).

APPENDIX B: THE RENORMALIZED COUPLING CONSTANTS OF THE EFFECTIVE HAMILTONIAN IN REGION (A)

The renormalization of coupling constants in region (A) (see Fig. 4) are given by the following equations. Some parameters have been defined in Appendix A.

$$J' = J\left(\frac{2}{2+q^2}\right)^2 (q^2 + 2J_2 q) + \frac{J^2}{4}\left(\frac{\Delta}{e_0 - e_2}\right)\left(\frac{q}{2+q^2}\right)^2$$
$$- \frac{J^2}{4}\left(\frac{1}{e_0 - e_1}\right)\left(\frac{1}{(2+q^2)(2+p^2)}\right)^2$$
$$\times (p+q)(pq)(p+q+4J_2)[4\Delta_2 - (\Delta + 2\Delta_2)pq]$$
$$- \frac{J^2}{4}\left(\frac{4}{2e_0 - e_1 - e_2}\right)\left(\frac{1}{2+q^2}\right)^2\left(\frac{q}{2+p^2}\right)(p+q+2J_2)$$
$$\times[\times 2\Delta_2 - (\Delta + \Delta_2)pq],$$

$$\Delta' = \left\{ J\left(\frac{q}{2+q^2}\right)^2 (\Delta q^2 - 2\Delta_2(2-q^2)) \right.$$
$$+ \frac{J^2}{4}\left(\frac{1}{e_0 - e_1}\right)\left(\frac{(p+q)^2 + 4J_2(p+q)}{(2+q^2)(2+p^2)}\right)^2$$
$$+ \frac{J^2}{4}\left(\frac{1}{e_0 - e_2}\right)\left(\frac{q^2}{2(2+q^2)}\right)^2 + \frac{J^2}{4}\left(\frac{1}{e_0 - e_3}\right)\left(\frac{1+2J_2 q}{2+q^2}\right)^2$$
$$+ \frac{J^2}{4}\left(\frac{2}{2e_0 - e_1 - e_2}\right)\left(\frac{1}{2+p^2}\right)\left(\frac{q(p+q+2J_2)}{2+q^2}\right)^2$$
$$- \frac{J^2}{4}\left(\frac{2}{2e_0 - e_2 - e_3}\right)\left(\frac{q(1+qJ_2)}{2+q^2}\right)^2 - \frac{J^2}{4}\left(\frac{4}{2e_0 - e_1 - e_3}\right)$$
$$\left. \times\left(\frac{J_2(pq+q^2+2)+p+q}{(2+q^2)(2+p^2)^{1/2}}\right)^2 \right\} \Big/ J',$$

$$J_2' = \left\{ \frac{J^2}{4}\left(\frac{2}{2+q^2}\right)^3 \left[\frac{[J_2(3q+p)+q(p+q)]^2}{(e_0 - e_1)(2+p^2)} \right.\right.$$
$$\left.\left. + \frac{[J_2(1+q^2)+q]^2}{e_0 - e_3} - \frac{(q^2 + J_2 q)^2}{2(e_0 - e_2)} \right] \right\} \Big/ J',$$

$$\Delta_2' = \left\{ \frac{J^2}{4}\left(\frac{2}{2+q^2}\right)^3 \left[\frac{\left(\Delta_2 q(p-pq^2+q) - \frac{\Delta}{2}pq^3\right)^2}{(e_0-e_1)(2+p^2)} - \frac{[-\Delta q^2 + \Delta_2(2-q^2)]^2}{2(e_0-e_2)} \right] \right\} \Big/ J'.$$

APPENDIX C: THE RENORMALIZED COUPLING CONSTANTS OF THE EFFECTIVE HAMILTONIAN IN REGION (B)

The renormalization of coupling constants in region (B) (see Fig. 4) are given by the following equations:

$$J' = \left(\frac{J}{4}\right)^2 \Delta \left[\left(\frac{1}{e_2-e_0}\right)\left(\frac{q}{2+q^2}\right)^2 + \left(\frac{1}{e_2-e_1}\right)\left(\frac{p}{2+p^2}\right)^2 + \left(\frac{4}{2e_2-e_1-e_0}\right)\left(\frac{q}{2+q^2}\right)\left(\frac{p}{2+p^2}\right) \right],$$

$$\Delta' = \left\{ \left(\frac{J}{4}\right)^2 \left[\left(\frac{1}{e_2-e_0}\right)\left(\frac{q^2}{2(2+q^2)}\right)^2 + \left(\frac{1}{e_2-e_1}\right)\left(\frac{p^2}{2(2+p^2)}\right)^2 + \left(\frac{1}{e_2-e_3}\right)\left(\frac{1}{4}\right) + \left(\frac{4}{2e_2-e_1-e_0}\right)\left(\frac{q^2}{2(2+q^2)}\right)\left(\frac{p^2}{2(2+p^2)}\right) - \left(\frac{2}{2e_2-e_3-e_0}\right)\left(\frac{q^2}{2(2+q^2)}\right) - \left(\frac{4}{2e_2-e_3-e_1}\right) \times \left(\frac{p^2}{2(2+p^2)}\right) \right] \right\} \Big/ J',$$

$$J_2' = \left\{ \left(\frac{JJ_2}{4}\right)^2 \left[\frac{2}{(e_2-e_0)}\left(\frac{q^2}{2(2+q^2)}\right) + \frac{2}{(e_2-e_1)}\left(\frac{p^2}{2(2+p^2)}\right) + \frac{2}{(e_2-e_3)}\left(\frac{1}{2}\right) \right] \right\} \Big/ J',$$

$$\Delta_2' = \left\{ \left(\frac{J\Delta_2}{4}\right)^2 \left[\frac{2}{(e_2-e_0)}\left(\frac{2}{2+q^2}\right) + \frac{2}{(e_2-e_1)}\left(\frac{2}{2+p^2}\right) \right] \right\} \Big/ J'.$$

[1] M. Hase, I. Terasaki, and K. Uchinokura, Phys. Rev. Lett. **70**, 3651 (1993).
[2] N. Motoyama, H. Eisaki, and S. Uchida, Phys. Rev. Lett. **76**, 3212 (1996).
[3] R. Coldea, D. A. Tennant, R. A. Cowley, D. F. McMorrow, B. Dorner, and Z. Tylczynski, Phys. Rev. Lett. **79**, 151 (1997).
[4] Y. Mizuno, T. Tohyama, S. Maekawa, T. Osafune, N. Motoyama, H. Eisaki, and S. Uchida, Phys. Rev. B **57**, 5326 (1998).
[5] S. F. Solodovnikov and Z. A. Solodovnikova, J. Struct. Chem. **38**, 765 (1997).
[6] M. Hase, H. Kuroe, K. Ozawa, O. Suzuki, H. Kitazawa, G. Kido, and T. Sekine, Phys. Rev. B **70**, 104426 (2004).
[7] J. des Cloizeaux and M. Gaudin, J. Math. Phys. **7**, 1384 (1966).
[8] K. Nomura and K. Okamoto, Phys. Lett. A **169**, 433 (1992).
[9] K. Nomura and K. Okamoto, J. Phys. A **27**, 5773 (1994).
[10] C. K. Majumdar and D. K. Ghosh, J. Math. Phys. **10**, 1388 (1969); J. Phys. C **3**, 911 (1970); J. Math. Phys. **10**, 1399 (1969).
[11] R. Bursill, G. A. Gehring, D. J. J. Farnell, J. B. Parkinson, T. Xiang, and C. Zeng, J. Phys.: Condens. Matter **7**, 8605 (1995).
[12] S. Hirata and K. Nomura, Phys. Rev. B **61**, 9453 (2000).
[13] S. R. White and I. Affleck, Phys. Rev. B **54**, 9862 (1996).
[14] R. Jafari and A. Langari, Physica A **364**, 213 (2006).
[15] D. C. Cabra, A. Honecker, and P. Pujol, Eur. Phys. J. B **13**, 55 (2000), and references therein.
[16] C. Itoi and S. Qin, Phys. Rev. B **63**, 224423 (2001).
[17] R. D. Somma and A. A. Aligia, Phys. Rev. B **64**, 024410 (2001).
[18] T. Hikihara, M. Kaburagi, and H. Kawamura, Phys. Rev. B **63**, 174430 (2001).
[19] T. Tonegawa and I. Harada, J. Phys. Soc. Jpn. **58**, 2902 (1989).
[20] V. Ya. Krivnov and A. A. Ovchinnikov, Phys. Rev. B **53**, 6435 (1996).
[21] D. V. Dmitriev and V. Ya. Krivnov, Phys. Rev. B **73**, 024402 (2006).
[22] A. V. Chubukov, Phys. Rev. B **44**, 4693 (1991).
[23] H. P. Bader and R. Schilling, Phys. Rev. B **19**, 3556 (1979).
[24] T. Hamada, J. Kane, S. Nakagawa, and Y. Nastume, J. Phys. Soc. Jpn. **57**, 1891 (1988); **58**, 3869 (1989).
[25] D. V. Dmitriev, V. Ya. Krivnov, and J. Richter, Phys. Rev. B **75**, 014424 (2007).
[26] D. Allen and D. Senechal, Phys. Rev. B **55**, 299 (1997).
[27] P. W. Anderson, Science **235**, 1196 (1987).
[28] A. A. Nersesyan, A. O. Gogolin, and F. H. L. Essler, Phys. Rev. Lett. **81**, 910 (1998).
[29] M. A. Martin-Delgado and G. Sierra, Int. J. Mod. Phys. A **11**, 3145 (1996).
[30] M. A. Martin-Delgado, arXiv:cond-mat/9610196 (unpublished).
[31] G. Sierra and M. A. Martin Delgado, *Strongly Correlated Magnetic and Superconducting Systems*, Lecture Notes in Physics Vo1. 478 (Springer, Berlin, 1997).
[32] A. Langari, Phys. Rev. B **58**, 14467 (1998); **69**, 100402(R) (2004).